

Article

Numerical Analysis of Nonlocal Optical Response of Metallic Nanoshells

Muhammad Khalid *  and Cristian Ciraci * 

Center for Biomolecular Nanotechnologies, Istituto Italiano di Tecnologia, Via Barsanti 14, 73010 Arnesano (LE), Italy

* Correspondence: muhammad.khalid@iit.it (M.K.); cristian.ciraci@iit.it (C.C.)

Received: 19 March 2019; Accepted: 5 April 2019; Published: 8 April 2019



Abstract: Nonlocal and quantum effects play an important role in accurately modeling the optical response of nanometer-sized metallic nanoparticles. These effects cannot be described by conventional classical theories, as they neglect essential microscopic details. Quantum hydrodynamic theory (QHT) has emerged as an excellent tool to correctly predict the nonlocal and quantum effects by taking into account the spatial dependence of the charge density. In this article, we used a QHT to investigate the impact of nonlocality and electron spill-out on the plasmonic behavior of spherical Na and Au nanoshells. We adopted a self-consistent way to compute the equilibrium charge density. The results predicted by QHT were compared with those obtained with the local response approximation (LRA) and the Thomas–Fermi hydrodynamic theory (TFHT). We found that nonlocal effects have a strong impact on both the near- and far-field optical properties of nanoshells, in particular, for the antibonding resonant mode. We also investigated the optical response of these systems for different thicknesses of the shell, both for Na and Au metals.

Keywords: Plasmonics; nanoshell; nonlocal response; hydrodynamic theory

1. Introduction

Electromagnetic wave interaction with metallic nanostructures shows distinctive properties resulting from the coupling of the incident light with the conduction electrons of the metal. The collective excitation of the conduction electrons is known as *surface plasmon*. Plasmon behavior of a metallic particle intrinsically depends on its shape and size, and a wise design can allow the ability to engineer optical signals at nanometer scale. Probing optical properties of metallic nanoparticles with different shapes and sizes has been a topic of significant experimental and theoretical interest [1–5]. When the geometric dimension of metallic particles is very small or the separation between extended structures is on the sub-nanometric scale, electromagnetic interactions cannot be accurately described in the framework of classical electrodynamics, that is, the local response approximation (LRA). In fact, in such systems, quantum mechanical effects, such as electron screening, spill-out, quantum tunneling, and size-dependent plasmon broadening, become important and cannot be captured by conventional local theories [6–13]. A common way to describe these nonlocal effects is by using *ab initio* approaches, such as time-dependent density functional theory (TDDFT) [14], however, this method can only deal with small size particles (a few nm in size) and its applicability to larger systems is hindered by the fact that the computational cost increases cubically with the number of electrons. To deal with the strongly-coupled multiscale plasmonic systems, many theoretical methods under different level of approximations have been proposed in the literature [15–22], among which quantum hydrodynamic theory (QHT) is very promising, as it can incorporate a wide range of effects, including quantum tunneling without neglecting retardation effects. Moreover, this method can also be extended to study full nonlinear electron dynamics [20–22]. Recently, QHT has been applied to study optical

properties of spherical nanomatryoshkas (core-shell nanostructures), and an excellent agreement with the microscopic calculations has been shown [23].

In this article, we will investigate nanometric metallic shell systems. Nanoshells are nanostructures offering very high tunability of plasmon resonances over a wide range of frequencies in the visible and infrared portion of the spectrum, a frequency regime of great interest for optical applications [24–26]. Metallic nanoshells consist of a dielectric core surrounded by a metal layer, usually gold or silver, such that their optical response is dramatically different from that of a solid metallic sphere [27,28]. Nanoshell structures exhibit two plasmon resonances, which can be seen as symmetric and antisymmetric coupling of plasmons supported by individual constituents, i.e., bare cavity and solid sphere [29,30]. These hybridized plasmon modes are also known as bonding (symmetric) and antibonding (antisymmetric) modes. Optical properties of nanoshells are determined by the plasmon resonances, which are very sensitive function of shell thickness. Due to very high tunability of the plasmon modes, nanoshell structures have attracted considerable attention and are very useful in many potential applications particularly in enhanced optical absorption [31], biosensing [32,33], surface-enhanced Raman scattering [34–36], biological analysis, and cancer therapy [37–39].

In this paper, we will relate our study of the nonlocal optical properties of Na and Au nanoshells with sub-nanometer shell thickness by using the state-of-the art quantum hydrodynamic theory and comparison of the results with LRA and Thomas–Fermi hydrodynamic theory (TFHT).

2. Quantum Hydrodynamic Theory

QHT equation of motion of an electronic system when coupled to Maxwell equations results in the following system of equations in frequency domain Reference [22]:

$$\nabla \times \nabla \times \mathbf{E} - \varepsilon_\infty \frac{\omega^2}{c^2} \mathbf{E} = \omega^2 \mu_0 \mathbf{P}, \quad (1)$$

$$-\frac{n_0 e}{m} \nabla \left(\frac{\delta G}{\delta n} \right)_1 + \frac{e}{m} \nabla \cdot \sigma^{(kxc)} - (\omega^2 + i\omega\gamma) \mathbf{P} = \frac{n_0 e^2}{m} \mathbf{E}, \quad (2)$$

where \mathbf{E} and \mathbf{P} represent the electric field and the polarization, respectively; μ_0 is the magnetic permeability, c is the speed of light in free-space, ω is the angular frequency, and ε_∞ is a local contribution to the permittivity of core electrons. $n_0(\mathbf{r})$ is the spatially dependent equilibrium charge density, γ is the phenomenological damping rate, and e and m indicate the electron charge and electron mass, respectively. $G[n]$ is the energy functional containing the total internal energy of the system and can be written as:

$$G[n] = T_{TF}[n] + T_{vW}[n] + E_{xc}[n], \quad (3)$$

where T_{TF} represents the kinetic energy in the Thomas–Fermi (TF) approximation and T_{vW} is the von Weizsäcker kinetic energy functional, a gradient dependent correction term added to the TF kinetic energy and E_{xc} indicates the exchange and correlation (XC) potential energy. $\sigma^{(kxc)}$ in Equation (2) is the viscoelastic kinetic-exchange-correlation tensor; it takes into account the nonlocal broadening of the plasmon energies [22]. $\left(\frac{\delta G}{\delta n} \right)_1$ is then the first-order term of the potential obtained by using the usual perturbation theory, considering $n = n_0 + n_1$, with n_0 the unperturbed equilibrium density and $n_1 = \nabla \cdot \mathbf{P}/e$ the first-order perturbation (linear term) of the charge density. Explicit mathematical expressions of the terms in Equation (2) have been presented in Reference [21,22]. If we neglect the viscoelastic term and the XC and von Weizsäcker energy functional in Equation (3), and assume a constant equilibrium charge density, i.e., $n_0(\mathbf{r}) = n_0$, Equation (3) reduces to the standard TFHT approximation. In this scenario, the first term in Equation (2) reduces to $\beta^2 \nabla(\nabla \cdot \mathbf{P})$ where the term β takes into account the electron pressure.

Under plane wave excitation, we solve Equations (1) and (2) for the vector fields \mathbf{E} and \mathbf{P} , which are further used to compute optical properties of the plasmonic nanoshells. It is important to remark, from a numerical point of view, that we solve Equation (2) only in the region of interest, i.e., a region

containing the nanoshell. Far enough ($\sim 30 a_0$, with a_0 being the Bohr radius) from the ion edge, where the equilibrium density, and hence, \mathbf{P} is practically zero (although not exactly since the electron density decays exponentially), we impose $\mathbf{P} = \mathbf{0}$. For numerical simulations, we used commercial software COMSOL Multiphysics [40], which allows a flexible implementation of Equation (1), (2). To ease the computational efforts in terms of memory and processing time, we exploited the symmetry of the geometry and used the so-called 2.5D technique for numerical simulations [41]. This method requires all fields to be written in terms of an azimuthal mode number m , such that a vector field \mathbf{v} can be written as: $\mathbf{v}(\rho, \phi, z) = \sum_{m \in \mathbb{Z}} \mathbf{v}^{(m)}(\rho, z) \exp[-im\phi]$, where $m \in \mathbb{Z}$. The advantage of this method is that an initially three-dimensional problem reduces to a few $(2m_{\max} + 1)$ two-dimensional problems. For sub-wavelength structures, $m_{\max} < 3$ is usually enough to accurately describe the problem.

3. Geometry of the Problem

We investigated the optical response of Na and Au spherical nanoshells with inner radius R_1 , outer radius R_2 , and shell thickness defined as $t_s = R_2 - R_1$, as shown in Figure 1. Plasmon modes of the nanoshell strongly depend on the shell thickness, dielectric constant of the core, and embedding medium [42]. For simplicity, we assume that the core and embedding medium is vacuum. It is interesting to notice that, in case of LRA (i.e., $G[n] = \sigma^{(kxc)} = 0$), Equation (1), (2) reduce to the Drude dielectric function of the form:

$$\varepsilon(\omega) = \varepsilon_\infty - \frac{\omega_p^2}{\omega(\omega + i\gamma)}, \tag{4}$$

where $\omega_p = \sqrt{e^2 n_0 / (m_e \varepsilon_0)}$. In the following, we take $\varepsilon_\infty = 1$ and $\gamma = 0.16$ eV for Na, and $\varepsilon_\infty = 8$ and $\gamma = 0.135$ for Au [23].

The nonlocal pressure term β defined in the TFHT can be expressed as: $\beta = \sqrt{3/5} v_F$, with v_F being the Fermi velocity of the electron where we take $v_F = 0.82 \times 10^6$ m/s for Na and $v_F = 1.39 \times 10^6$ m/s for Au.

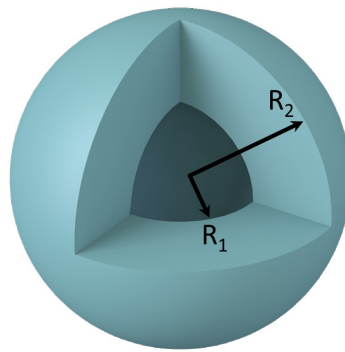


Figure 1. Spherical nanoshell with inner radius R_1 and outer radius R_2 .

For the QHT case, we modeled the nanoshells with Jellium approximation [43,44], in which a uniform background positive charge $n^+ = (r_s^3 4\pi/3)^{-1}$ confines electrons in the metal; where r_s is the Wigner–Seitz radius that is $r_s = 3 a_0$ for Au and $r_s = 4 a_0$ for Na. We compute the equilibrium electron density self-consistently by using the following nonlinear differential Equation [22],

$$\nabla^2 \left(\frac{\partial G[n]}{\partial n} \right)_{n=n_0} + \frac{e^2}{\varepsilon_0} (n_0 - n^+) = 0, \tag{5}$$

where ε_0 is the permittivity of the free-space. Equation (5) is obtained by combining the zero-*th* order QHT equation and the Poisson equation for the electrostatic potential [22]. The space-dependence of the ground-state density $n_0(\mathbf{r})$ is very crucial in characterizing the optical response of nanoplasmonic systems. In order to compute the unperturbed electron density $n_0(\mathbf{r})$ of the nanoshells, we considered

the following expression as an initial guess (similar to Reference [21] for spheres and to Reference [23] for spherical nanomatryoshkas):

$$n_{0\text{guess}}(\mathbf{r}) = \left(\frac{1}{1 + \exp[\kappa_1(R_1 - r)]} \right) \times \left(\frac{1}{1 + \exp[-\kappa_2(R_2 - r)]} \right), \quad (6)$$

where r indicates the distance from the center of the nanoshell and κ_1 and κ_2 represent the asymptotic decay of the electron density from the inner and outer surfaces of the shell, respectively. The solution is then found by solving Equation (5) iteratively.

4. Numerical Results and Discussion

This section presents numerical results for Na and Au nanoshells. Optical response of noble metals such as gold or silver could be complicated to analyze due to interband transitions. Therefore, we first perform simulations for Na, which is a simple Drude-like material and then extrapolate the understanding to analyze the behavior of Au nanoshell. Na is also interesting to study in a sense that it has lower work function and the spill-out is more pronounced as the electrons are more relaxed at the surface [23]. We take the nanostructure with a fixed vacuum core $R_1 = 2$ nm and different shell thicknesses, t_s , ranging from 0.5 nm to 10 nm placed in vacuum. A systematic comparison between local, TFHT and QHT approximations is shown. We consider a plane-wave excitation incident on the nanoparticle.

4.1. Na Nanoshell

Absorption spectra for Na nanoshell with $t_s = 0.5$ nm ($R_1 = 2$ nm, $R_2 = 2.5$ nm) computed using different approaches are shown in Figure 2a. It can be clearly seen that for this particular geometrical parameters, the two plasmon modes supported by nanoparticle are well separated in all three cases. In fact, for a nanoshell, the hybridization of the plasmon modes and splitting between them depend upon the shell thickness. It has been shown that according to classical electrodynamics, if the shell thickness is very small, the cavity and sphere plasmons have a strong interaction and the resulting hybridized modes supported by the shell structure are very well-separated. However, by increasing the shell thickness and eventually increasing the metal content of the shell, the bonding mode occurring at the lower energy takes a blue shift and the antibonding mode occurring at higher energy moves towards the red side of the spectrum [45,46]. Figure 2a, depicting the absorption spectra for Na nanoshell, shows that the local response theory predicts lower energy (bonding) mode, resulting from the symmetric coupling of sphere-cavity modes, at 2.07 eV and higher energy (antibonding) mode, resulting from the antisymmetric coupling, at 5.51 eV. In Thomas–Fermi approximation, the low-energy mode (LEM) is slightly blue shifted by 0.07 eV (at 2.14 eV) while the high-energy mode (HEM) shows relatively large shift by 1.03 eV (at 6.54 eV) towards higher energies with respect to LRA. QHT predicts LEM at 2.12 eV slightly blue shifted with respect to LRA and red shifted with respect to TFHT while a fairly large red shift for the HEM (at 4.89 eV) as compared to both LRA and TFHT.

The shift in the plasmon resonances given by the TFHT and QHT with respect to LRA is due to nonlocal effects. Time-dependent DFT calculations reported in the literature [47] have shown that, due to quantum mechanical effects, the plasmon resonance of Na nanostructures undergoes a red shift, which is associated with the electron spill-out from the metal surface into the free space [20–23,47]. On the contrary, the TFHT predicts a blue shift with respect to the LRA in the plasmon energies of Na nanoparticles which comes from the presence of the electron pressure, that is, the induced charges are pushed inwards into the bulk metal [48]. TFHT, however, overlooks the essential quantum effects such as electron spill-out and tunneling. The shifts in the plasmon resonances in the case of nanoshell can also be elaborated in terms of the effective size of the nanoparticle [48]. In QHT, due to electron spill-out, the effective size or thickness of the nanoshell looks larger than its physical thickness which causes the LEM to move towards higher energy and the HEM to the lower energy with respect to LRA. For the case of TFHT which overlooks the spill-out and takes into account the electron pressure, the

effective thickness of the nanoshell becomes smaller than the physical thickness resulting in a blue shift in the surface plasmon modes with respect to LRA. We note that the nonlocal or quantum effects strongly influence the antibonding mode as compared to the bonding mode.

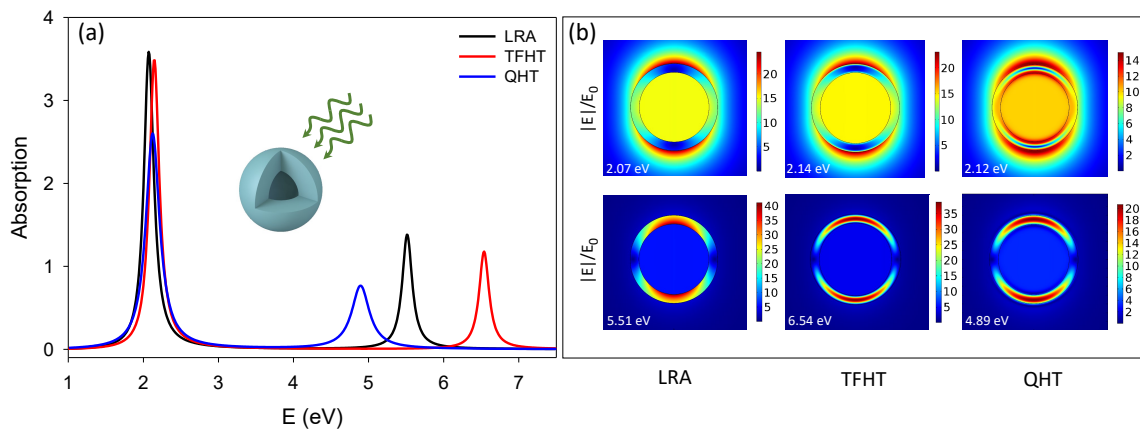


Figure 2. (a) Absorption efficiency of Na nanoshell with $R_1 = 2$ nm and $R_2 = 2.5$ nm calculated using local response approximation (LRA), Thomas–Fermi hydrodynamic theory (TFHT), and quantum hydrodynamic theory (QHT). (b) Electric field distribution plotted at corresponding resonance frequencies, both at lower (upper panel) and higher energy modes (lower panel), computed using different methods.

Electric field distribution for the Na nanoshell discussed above is depicted in Figure 2b both at lower and higher energy modes at the corresponding resonance frequencies. The electric distribution and enhancement directly depend on the electron confinement and spill-out, reiterating that these quantities show substantial dependence on the charge density profile. It can be noticed that the electric field enhancement given by QHT is much lower than the LRA and TFHT approximations. Since LRA and TFHT assume that the electrons cannot escape the metal surface, therefore, the field is discontinuous at the metal boundaries. The effect of electron pressure in the TFHT case can also be seen whereas QHT shows a continuous field distribution as it takes into account the space dependence of the electron density.

In the following, we discuss the ground-state and induced charge density for the Na nanoshell. It has been reported previously for sphere [22] and core-shell nanostructures [23] that equilibrium and induced charge density calculated within QHT shows a good agreement with the TD-DFT results. Despite the fact that QHT does not fully incorporate the wave nature of electrons due to approximate energy functional and consequently neglecting the quantum (Friedel) oscillations inside the metal, however, it describes the charge density with a high accuracy near the metal surface, which is the region of utmost interest. The ground-state density is obtained by solving Equation (5) self-consistently and the induced-charge density $n_1 = \nabla \cdot \mathbf{P}/e$. The real and imaginary parts of the induced charge density along with the equilibrium density at lower and higher energy modes are shown in Figure 3a,b, respectively. The shaded grey area represents the metal region and the insets show the color maps for real and imaginary parts. A prominent spill-out from the metal boundaries can be clearly seen and this nonlocal spill-out can be very crucial and directly influences the far-field optical properties, as was seen in Figure 2.

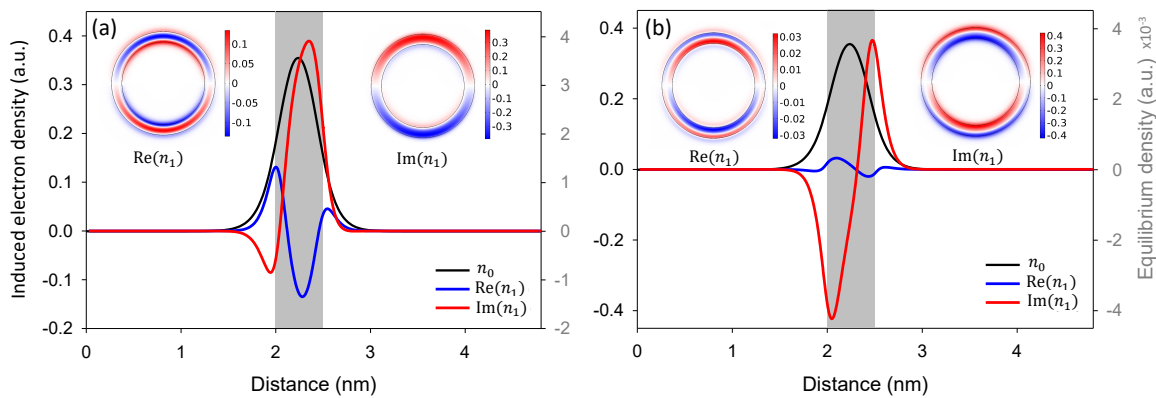


Figure 3. Induced electron density n_1 and ground-state density n_0 for Na nanoshell with $t_s = 0.5$ nm at (a) low-energy mode (LEM) and (b) high-energy mode (HEM). The insets show the map plots for real and imaginary part of the induced density.

Since the thickness of the shell considered in Figure 3 is very small $t_s = 0.5$ nm, the charge density is nowhere flat due to significant spill-out. In Figure 4a, we report equilibrium and induced charge density for Na nanoshell with shell thickness $t_s = 3$ nm ($R_1 = 2$ nm and $R_2 = 5$ nm). In this case, the equilibrium charge density is constant inside the metal except near the metal interfaces where a considerable spill-in and spill-out from the metal surfaces can be observed. The two oscillations in the ground-state density inside the metal near the interfaces are reminiscent of Friedel oscillations.

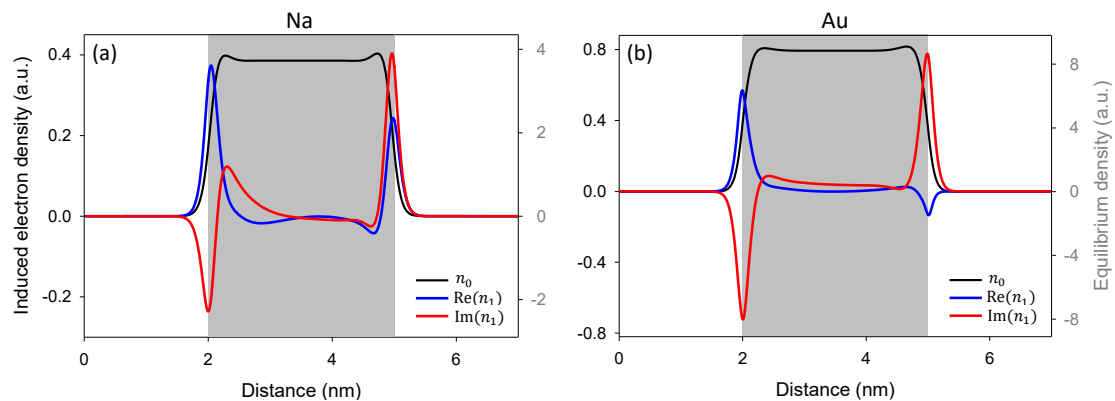


Figure 4. Equilibrium density n_0 and real and imaginary parts of the induced charge density n_1 for (a) Na and (b) Au nanoshell with shell thickness $t_s = 3$ nm ($R_1 = 2$ nm and $R_2 = 5$ nm).

Figure 5a–c shows absorption spectra for Na nanoshell for various shell thicknesses while keeping the core radius constant. We report a systematic comparison between the LRA, TFHT, and QHT approximations. For small shell thicknesses, the plasmon resonances are well-separated. When the shell thickness is increased, as we discussed in the first paragraph of this section, LRA shows that the LEM moves towards higher energy while the HEM mode moves in the opposite direction, i.e., towards lower energies. The shift in LEM with increasing thickness is much higher than the HEM, as can be seen in Figure 5a. A similar behavior is predicted by the TFHT with increasing shell thickness, however, with reference to LRA it shows a blue shift for both plasmon modes. The shift is strong for the HEM as compared to LEM particularly for smaller shell thicknesses. According to QHT, as the shell thickness grows the LEM mode shifts towards higher energies and the HEM diminishes abruptly. It is worthy to note that the nonlocal or quantum effects influence the HEM in a dramatic manner. Even for a slight increase in the shell thickness, the amplitude of the LEM decreases very rapidly and the mode completely disappears for $t_s \geq 2$ nm. This can be explained in the following: according to the classical theory, when the shell thickness is increased the interaction between cavity and sphere plasmons gets weaker, thus, decreasing the strength of antibonding mode. When the shell

is sufficiently thick, the cavity resonance is not excited by the incident field and the shell behaves like a solid sphere. For the QHT case, we can say that even for the relatively smaller shell thickness, the antibonding mode disappears because of the effective size of the shell appears relatively bigger due to spill-out effect which weakens the cavity mode and the nonlocal broadening causes significant damping. Moreover, the viscoelastic tensor introduces an extra broadening that further damps the antibonding mode.

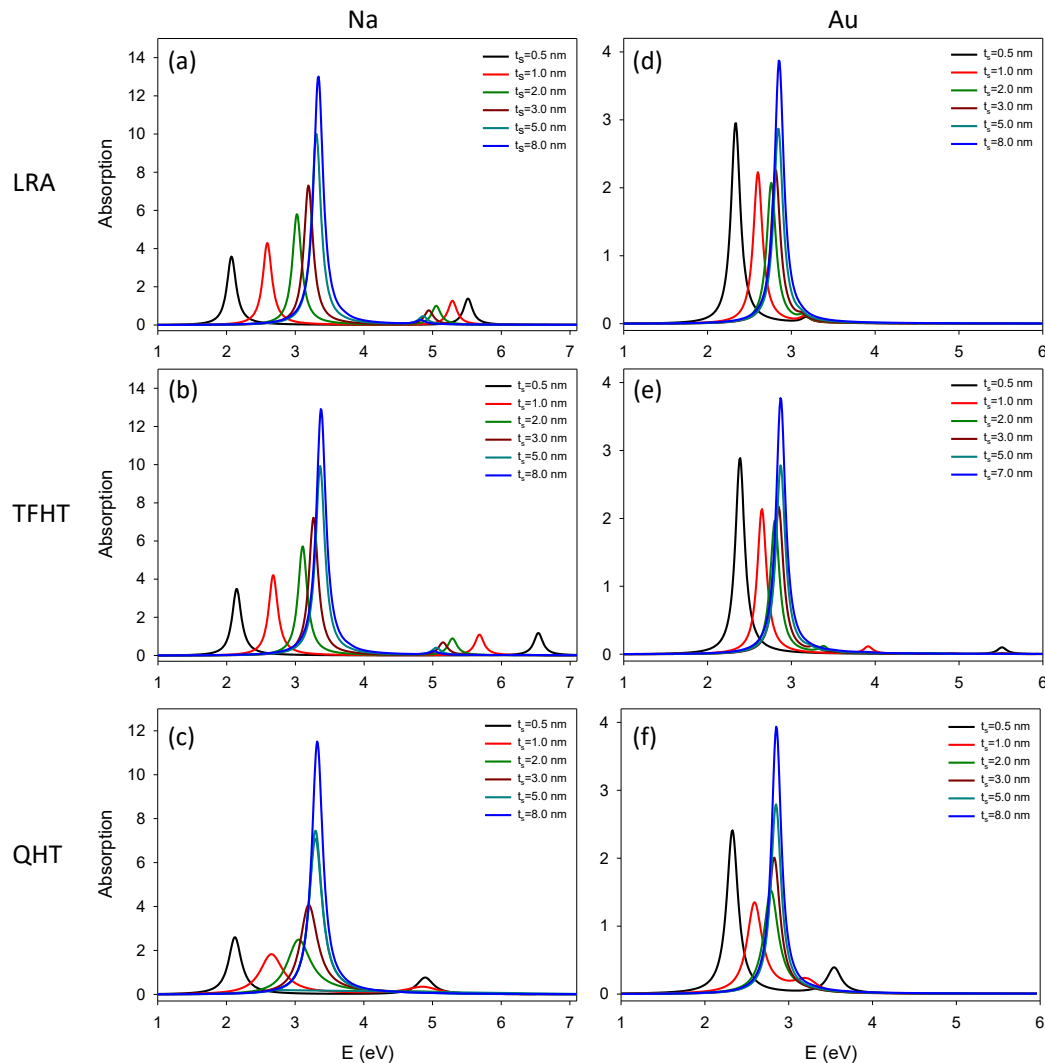


Figure 5. Absorption spectra for Na (left panel) and Au (right panel) nanoshell calculated within different theories for different shell thicknesses $t_s = R_2 - R_1$ with a fixed core radius $R_1 = 2$ nm.

We know that the nonlocal effects have a strong impact on the antibonding mode (HEM) and a little on the bonding mode (LEM). Since this slight shift in the LEM due to nonlocal effects predicted by TFHT and QHT methods as compared to LRA is not very clear in Figure 5a, therefore, in the following we present a comparison of plasmon energies at this mode for the aforesaid approaches. Figure 6a shows the resonance energies at the LEM for Na nanoshell as a function of shell thickness predicted by different approaches. For smaller thickness, QHT predicts a slight blue shift with respect to LRA and red shift with respect to TFHT. We can see that for higher shell thickness QHT and LRA matches well whereas TFHT shows a slight blue shift.

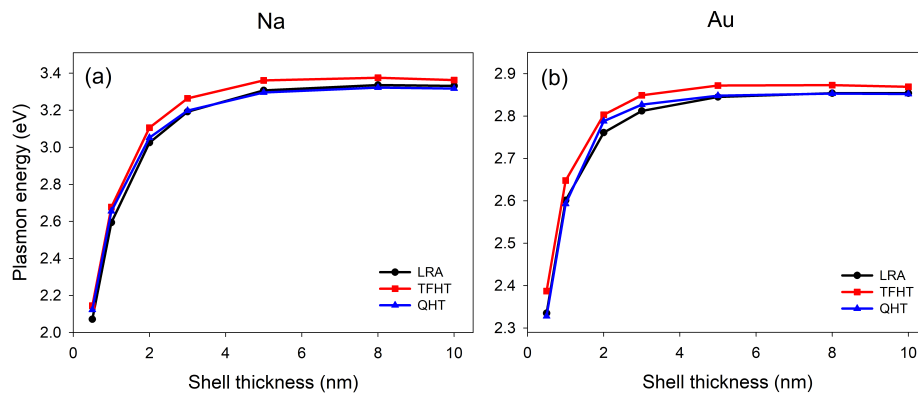


Figure 6. Plasmon energy of LEM for (a) Na and (b) Au nanoshell as a function of shell thickness $t_s = R_2 - R_1$ and with a fixed core radius $R_1 = 2$ nm. Results predicted by different methods are presented.

4.2. Au Nanoshell

Now we consider Au nanoshell to analyze the nonlocal optical properties for various shell thicknesses using different techniques. We conduct a similar study as presented in the previous part of this section. However, Au cannot be described by simple Drude model and the electron response of Au is somewhat complicated as compared to Na, due to the contribution of the d-band electron transitions and background core permittivity ϵ_∞ . The absorption spectra for Au nanoshell with 0.5 nm shell thickness computed within LRA, TFHT, and QHT methods are shown in Figure 7a. It has been shown in Reference [45] within the framework of local response theory that the presence of ϵ_∞ produces a strong red shift in the antibonding (HEM) mode. This is why we see in Figure 7a that the two plasmon modes given by LRA are not very well-separated as much as was seen in the case of Na nanoshell because the HEM is pushed to lower energies due to the presence of background core charges. If we neglect the contribution from the core charges ($\epsilon_\infty = 1$), the antibonding mode will get a strong shift to the higher energies. Nonlocal optical properties of nanoshell structures have been extensively studied in the literature within the framework of TFHT and the shift of both plasmon modes of a nanoshell towards higher energies as compared to local description has already been reported [49–52]. It has also been shown that TFHT predicts a strong blue shift for the antibonding mode with respect to LRA [53,54]. Figure 7a displays that the TFHT predicts a little blue shift for the LEM and a very large blue shift for the HEM with respect to LRA in the spectrum of the nanoshell. The QHT predicts that the LEM is more or less at the same energy as given by LRA whereas the HEM is blue shifted with respect to LRA and red shifted with respect to TFHT. This blue shift in the plasmon resonance is associated with the optical interband transitions in the noble metals, as seen in several nanostructures of different configurations [6–8].

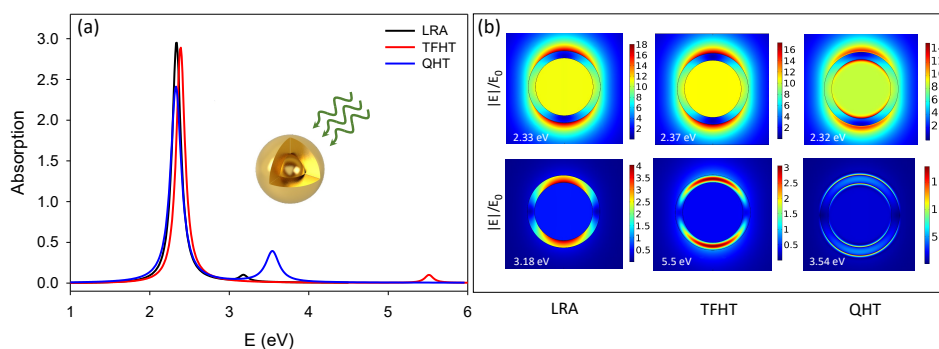


Figure 7. (a) Absorption efficiency of Au nanoshell with $R_1 = 2$ nm and $R_2 = 2.5$ nm calculated using LRA, TFHT, and QHT. (b) Electric field distribution plotted at corresponding resonance frequencies both at lower (upper panel) and higher energy modes (lower panel) computed using different methods.

The electric field distribution predicted by different theories for Au nanoshell with shell thickness 0.5 nm both at LEM and HEM at the corresponding resonance frequency is shown in Figure 7b. It is interesting to notice that differently from Na nanoshells, this time also in the QHT case the fields are discontinuous at the metal boundaries and the LEM shows a strong field near the metal surface. These effects are due to a non-zero contribution of the local polarizability contribution given by core electrons and described through ϵ_∞ .

Figure 8 plots the induced charge density along with the ground-state density at LEM and HEM for Au nanoshell with 0.5 nm shell thickness. Let us recall that the equilibrium charge density is computed by using Equation (5) and the induced-charge density by the relation $n_1 = \nabla \cdot \mathbf{P}/e$. The color-map plots for the real and imaginary parts of induced charge density are shown in the insets and the shaded grey regions represent the metal. As the shell thickness is very small (0.5 nm), again in this case, the charge density is nowhere flat and a significant spill-out from the metal surfaces of the shell can be noted. The equilibrium and induced charge density for Au nanoshell with $t_s = 3$ nm ($R_1 = 2$ nm and $R_2 = 5$ nm) at the corresponding resonance is shown in Figure 4b. As the metal content in this case is relatively large, therefore, the equilibrium density is constant inside the bulk region and a considerable electron spill-out from the metal surfaces into free-space can be seen.

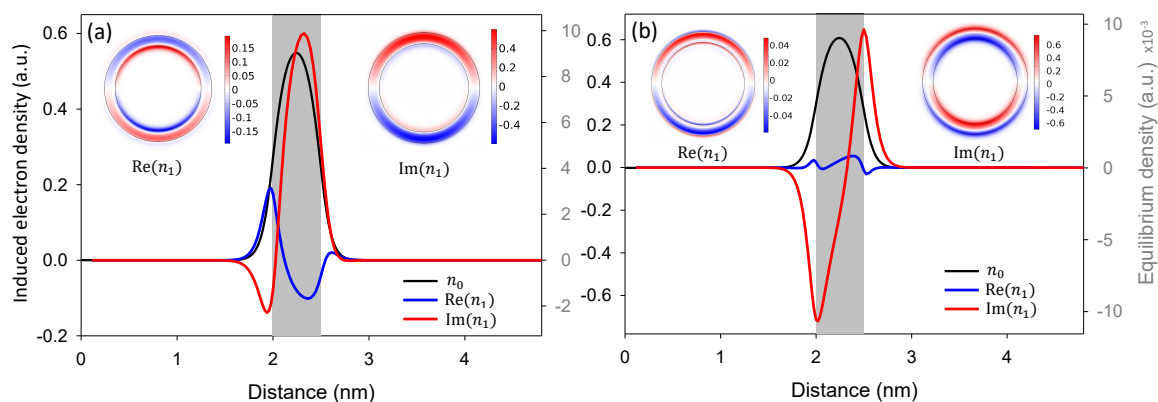


Figure 8. Induced electron density for Au nanoshell at (a) LEM and (b) HEM. The insets show the map plots for real and imaginary part of the induced density.

Now we study the optical behavior of the nanoshell for increasing shell thickness while keeping the core radius constant. The absorption spectra for Au nanoshell for various shell thicknesses are shown in Figure 5d–f. LRA results show that as the shell thickness increases the LEM undergoes towards higher energies and the HEM moves slightly to lower energies. The coupling between cavity plasmons and sphere plasmons decreases as the thickness increases. For larger shell thickness the LEM and HEM overlap resulting into a single plasmon resonance and it happens when $t_s > 5$ nm, where no cavity plasmons are excited and the nanoshell acts as a solid sphere. The TFHT shows a strong blueshift for the HEM with respect to local calculations and with increasing shell thickness this mode abruptly shifts to the lower energy and finally coincide completely with the LEM for $t_s > 5$ nm. In case of QHT, we see that the HEM disappears much faster as compared to other methods and it vanishes entirely for $t_s > 1$ nm due to nonlocal or quantum effects.

As we saw in the case of Na nanoshell that nonlocal effects substantially influence the antibonding plasmon mode; similarly, for the case of Au, HEM is strongly affected whereas the impact of nonlocal effects on the LEM is minor. In order to show to the reader more clearly the trend of this shift predicted by different methods, we plot in Figure 6b the resonance energies at the LEM for Au nanoshell as a function of shell thickness. QHT predicts the plasmon resonance almost at the same energy as given by LRA, whereas, TFHT shows a blue shift with respect to QHT and LRA.

5. Conclusions

In this paper, we presented a numerical analysis of nonlocal optical properties of Na and Au nanoshells for various shell thicknesses. We used state-of-the-art quantum hydrodynamic theory to study nonlocal effects in these nanostructures and compared this approach systematically with the local response and Thomas–Fermi approximations both for Na and Au metals. We noted that QHT predicts a significant electron spill-out from the metal surfaces and this nonlocal spill-out has a strong impact particularly on the antibonding resonant mode (HEM). The HEM shows a noteworthy red shift for Na nanoshell and blue shift for Au nanoshell as compared to local response theory. Therefore, it is very important to take into account these quantum effects in properly designing metallic nanoshells with specific plasmon energies and in accurately describing their near-field as well as far-field plasmonic response.

Author Contributions: The authors have equal contribution to this work.

Funding: This research was funded by the Air Force Office of Scientific Research under award number FA9550-17-1-0177.

Conflicts of Interest: The authors declare no conflict of interest.

Abbreviations

The following abbreviations are used in this manuscript:

LRA	Local response approximation
TFHT	Thomas–Fermi hydrodynamic theory
QHT	Quantum hydrodynamic theory
LEM	Lower energy mode
HEM	Higher energy mode

References

1. Kreibig, U.; Vollmer, M. *Optical Properties of Metal Clusters*; Springer: Heidelberg, Germany, 1995.
2. Kelly, K.L.; Coronado, E.; Zhao, L.L.; Schatz, G.C. The optical properties of metal nanoparticles: The influence of size, shape and dielectric environment. *J. Phys. Chem. B* **2003**, *107*, 668–677. [[CrossRef](#)]
3. Yu, Y.-Y.; Chang, S.-S.; Lee, C.-L.; Wang, C.R.C. Gold nanorods: Electrochemical synthesis and optical properties. *J. Phys. Chem. B* **1997**, *101*, 6661–6664. [[CrossRef](#)]
4. Jin, R.; Cao, Y.; Mirkin, C.A.; Kelly, K.L.; Schatz, G.C.; Zheng, J.G. Photoinduced conversion of silver nanospheres to nanoprisms. *Science* **2001**, *294*, 1901–1903. [[CrossRef](#)] [[PubMed](#)]
5. Sun, Y.; Xia, Y. Shape-controlled synthesis of gold and silver nanoparticles. *Science* **2002**, *298*, 2176–2179. [[CrossRef](#)]
6. Raza, S.; Toscano, G.; Jauho, A.P.; Wubs, M.; Mortensen, N.A. Unusual resonances in nanoplasmonic structures due to nonlocal response. *Phys. Rev. B* **2011**, *84*, 121412. [[CrossRef](#)]
7. Raza, S.; Bozhevolnyi, S.I.; Wubs, M.; Mortensen, N.A. Nonlocal optical response in metallic nanostructures. *J. Phys.: Condens. Matter* **2015**, *27*, 183204. [[CrossRef](#)]
8. Toscano, G.; Raza, S.; Jauho, A.P.; Mortensen, N.A.; Wubs, M. Modified field enhancement and extinction by plasmonic nanowire dimers due to nonlocal response. *Opt. Express* **2012**, *20*, 4176–4188. [[CrossRef](#)] [[PubMed](#)]
9. Ciraci, C.; Hill, R.T.; Mock, J.J.; Urzhumov, Y.; Fernández-Domínguez, A.I.; Maier, S.A.; Pendry, J.B.; Chilkoti, A.; Smith, D.R. Probing the ultimate limits of plasmonic enhancement. *Science* **2012**, *337*, 1072–1074. [[CrossRef](#)]
10. Ciraci, C.; Urzhumov, Y.A.; Smith, D.R. Effects of classical nonlocality on the optical response of three-dimensional plasmonic nanodimers. *J. Opt. Soc. Am. B* **2013**, *30*, 2731–2736. [[CrossRef](#)]
11. Zhu, W.; Esteban, R.; Borisov, A.G.; Baumberg, J.J.; Nordlander, P.; Lezec, H.J.; Aizpurua, J.; Crozier, K.B. Quantum mechanical effects in plasmonic structures with subnanometre gaps. *Nat. Commun.* **2016**, *7*, 11495. [[CrossRef](#)]

12. Savage, K.J.; Hawkeye, M.M.; Esteban, R.; Borisov, A.G.; Aizpurua, J.; Baumberg, J.J. Revealing the quantum regime in tunneling plasmonics. *Nature* **2012**, *491*, 574–577. [[CrossRef](#)] [[PubMed](#)]
13. Scholl, J.A.; García-Etxarri, A.; Koh, A.L.; Dionne, J.A. Observation of quantum tunneling between two plasmonic nanoparticles. *Nano Lett.* **2013**, *13*, 564–569. [[CrossRef](#)]
14. Ullrich, C.A. *Time-Dependent Density Functional Theory: Concepts and Applications*; Oxford University Press: Oxford, UK, 2011.
15. Lermé, J.; Palpant, B.; Cottancin, E.; Pellarin, M.; Prével, B.; Vialle, J.L.; Broyer, M.; Quantum extension of mie's theory in the dipolar approximation. *Phys. Rev. B* **1999**, *60*, 16151–16156. [[CrossRef](#)]
16. Esteban, R.; Borisov, A.G.; Nordlander, P.; Aizpurua, J. Bridging quantum and classical plasmonics with a quantum-corrected model. *Nat. Commun.* **2012**, *3*, 825. [[CrossRef](#)]
17. Luo, Y.; Fernández-Domínguez, A.I.; Wiener, A.; Maier, S.A.; Bendry, J.B. Surface plasmons and nonlocality: A simple model. *Rev. Mod. Phys.* **2013**, *111*, 093901. [[CrossRef](#)]
18. Yan, W.; Wubs, M.; Mortensen, N.A. Projected dipole model for quantum plasmonics. *Phys. Rev. Lett.* **2015**, *115*, 137403. [[CrossRef](#)] [[PubMed](#)]
19. Zapata, M.; Beltrán, A.S.C.; Borisov, A.G.; Aizpurua, J. Quantum effects in the optical response of extended plasmonic gaps: Validation of the quantum corrected model in core-shell nanomatryushkas. *Opt. Express* **2015**, *23*, 8134–8149. [[CrossRef](#)]
20. Toscano, G.; Straubel, J.; Kwiatkowski, A.; Rockstuhl, C.; Evers, F.; Xu, H.; Mortensen, N.A.; Wubs, M. Resonance shifts and spill-out effects in self-consistent hydrodynamic nanoplasmonics. *Nat. Commun.* **2015**, *6*, 7132. [[CrossRef](#)]
21. Ciraci, C.; Sala, F.D. Quantum hydrodynamic theory for plasmonics: Impact of the electron density tail. *Phys. Rev. B* **2016**, *93*, 205405. [[CrossRef](#)]
22. Ciraci, C. Current-dependent potential for nonlocal absorption in quantum hydrodynamic theory. *Phys. Rev. B* **2017**, *95*, 245434. [[CrossRef](#)]
23. Khalid, M.; Sala, F.D.; Ciraci, C. Optical properties of plasmonic core-shell nanomatryoshkas: A quantum hydrodynamic analysis. *Opt. Express* **2018**, *26*, 17322–17334. [[CrossRef](#)]
24. Oldenburg, S.J.; Averitt, R.D.; Westcott, S.L.; Halas, N.J. Nanoengineering of optical resonances. *Chem. Phys. Lett.* **1998**, *288*, 243–247. [[CrossRef](#)]
25. Oldenburg, S.J.; Jackson, J.B.; Westcott, S.L.; Halas, N.J. Infrared extinction properties of gold nanoshells. *Appl. Phys. Lett.* **1999**, *75*, 2897–2899. [[CrossRef](#)]
26. Aizpurua, J.; Hanarp, P.; Sutherland, D.S.; Kall, M.; Bryant, G.W.; de Abajo, F.J.G. Optical properties of gold nanorings. *Phys. Rev. Lett.* **2003**, *90*, 57401. [[CrossRef](#)]
27. Averitt, R.D.; Sarkar, D.; Halas, N.J. Plasmon resonance shifts of Au-coated Au₂S nanoshells: Insight into multicomponent nanoparticle growth. *Phys. Rev. Lett.* **1997**, *78*, 4217–4220. [[CrossRef](#)]
28. Prodan, E.; Nordlander, P.; Halas, N.J. Effects of dielectric screening on the optical properties of metallic nanoshells. *Chem. Phys. Lett.* **2003**, *368*, 94–101. [[CrossRef](#)]
29. Prodan, E.; Radloff, C.; Halas, N.J.; Nordlander, P. A hybridization model for the plasmon response of complex nanostructures. *Science* **2003**, *302*, 419–422. [[CrossRef](#)]
30. Prodan, E.; Nordlander, P. Plasmon hybridization in spherical nanoparticles. *J. Chem. Phys.* **2004**, *120*, 5444–5454. [[CrossRef](#)]
31. Baer, R.; Neuhauser, D.; Weiss, S. Enhanced absorption induced by a metallic nanoshell. *Nano Lett.* **2004**, *4*, 85–88. [[CrossRef](#)]
32. West, J.L.; Halas, N.J. Engineered nanomaterials for biophotonics application: Improving sensing, imaging, and therapeutics. *Annu. Rev. Biomed. Eng.* **2003**, *5*, 285–292. [[CrossRef](#)]
33. Khlebtsov, B.N.; Khlebtsov, N.G. Biosensing potential of silica/gold nanoshells: Sensitivity of plasmon resonance to the local dielectric environment. *J. Quant. Spectr. Radiat. Trans.* **2007**, *106*, 154–169. [[CrossRef](#)]
34. Oldenburg, S.J.; Westcott, S.L.; Averitt, R.D.; Halas, N.J. Surface enhanced Raman scattering in the near infrared using metal nanoshell substrates. *J. Chem. Phys.* **1999**, *111*, 4729–4735. [[CrossRef](#)]
35. Hao, E.; Li, S.; Bailey, S.L.; Zou, S.; Schatz, G.C.; Hupp, J.T. Optical properties of metal nanoshells. *J. Phys. Chem. B* **2004**, *108*, 1224–1229. [[CrossRef](#)]
36. Goude, Z.E.; Leung, P.T. Surface enhanced Raman scattering from metallic nanoshells with nonlocal dielectric response. *Solid State Commun.* **2007**, *143*, 416–420. [[CrossRef](#)]

37. Hirsch, L.R.; Stafford, R.J.; Bankson, J.A.; Sershen, S.R.; Rivera, B.; Price, R.E.; Hazle, J.D.; Halas, N.J.; West, J.L. Nanoshell-mediated near-infrared thermal therapy of tumors under magnetic resonance guidance. *Proc. Natl. Acad. Sci. USA* **2003**, *100*, 13549–13555. [[CrossRef](#)]
38. Khlebtsov, B.; Zharov, V.; Melnikov, A.; Tuchin, V.; Khlebtsov, N. Optical amplification of photothermal therapy with gold nanoparticles and nanoclusters. *Nanotechnology* **2006**, *17*, 5167–5179. [[CrossRef](#)]
39. Harris, N.; Ford, M.J.; Cortie, M.B. Optimization of plasmonic heating by gold nanospheres and nanoshells. *J. Phys. Chem. B* **2006**, *110*, 10701–10707. [[CrossRef](#)]
40. COMSOL Multiphysics. Available online: <http://www.comsol.com> (accessed on 7 April 2019).
41. Ciraci, C.; Urzhumov, Y.A.; Smith, D.R. Far-field analysis of axially symmetric three-dimensional directional cloaks. *Opt. Express* **2013**, *21*, 9397–9406. [[CrossRef](#)]
42. Prodan, E.; Lee, A.; Nordlander, P. The effect of a dielectric core and embedding medium on the polarizability of metallic nanoshells. *Chem. Phys. Lett.* **2002**, *360*, 325–332. [[CrossRef](#)]
43. Ekardt, W. Size-dependent photoabsorption and photoemission of small metal particles. *Phys. Rev. B* **1985**, *31*, 6360–6370. [[CrossRef](#)]
44. Brack, M. The physics of simple metal clusters: Self-consistent jellium model and semiclassical approaches. *Rev. Mod. Phys.* **1993**, *65*, 677–732. [[CrossRef](#)]
45. Prodan, E.; Nordlander, P. Structural tunability of the plasmon resonances in metallic nanoshells. *Nano Lett.* **2003**, *3*, 543–547. [[CrossRef](#)]
46. Shayesteh, S.F.; Saie, M. The effect of surface plasmon resonance on optical response in dielectric (core)-metal (shell) nanoparticles. *Pramana-J. Phys.* **2015**, *85*, 1245–1255. [[CrossRef](#)]
47. Zuloaga, J.; Prodan, E.; Nordlander, P. Quantum description of the plasmon resonances of a nanoparticle dimer. *Nano Lett.* **2009**, *9*, 887–891. [[CrossRef](#)]
48. Teperik, T.V.; Nordlander, P.; Aizpurua, J.; Borisov, A.G. Robust Subnanometric plasmon ruler by rescaling of the nonlocal optical response. *Phys. Rev. Lett.* **2013**, *110*, 263901. [[CrossRef](#)] [[PubMed](#)]
49. Rojas, R.; Claro, F.; Fuchs, R. Nonlocal response of a small coated sphere. *Phys. Rev. B* **1988**, *37*, 6799–6807. [[CrossRef](#)]
50. David, C.; de Abajo, J.G. Spatial nonlocality in the optical response of metal nanoparticles. *J. Phys. Chem. C* **2011**, *115*, 19470–19475. [[CrossRef](#)]
51. Huang, Y.; Goa, L. Superscattering of light from core-shell nonlocal plasmonic nanoparticles. *J. Phys. Chem. C* **2014**, *118*, 30170–30178. [[CrossRef](#)]
52. Huang, Y.; Xiao, J.J.; Goa, L. Antibonding and bonding lasing modes with low gain threshold in nonlocal metallic nanoshell. *Opt. Express* **2015**, *23*, 8818–8828. [[CrossRef](#)]
53. Tserkezis, C.; Gantzounis, G.; Stefanou, N. Collective plasmonic modes in ordered assemblies of metallic nanoshells. *J. Phys.: Condens. Matter* **2008**, *20*, 075232. [[CrossRef](#)]
54. Tserkezis, C.; Stefanou, N.; Wubs, M.; Mortensen, N.A. Molecular fluorescence enhancement in plasmonic environments: Exploring the role of nonlocal effects. *Nanoscale* **2016**, *8*, 17532–17541. [[CrossRef](#)] [[PubMed](#)]



© 2019 by the authors. Licensee MDPI, Basel, Switzerland. This article is an open access article distributed under the terms and conditions of the Creative Commons Attribution (CC BY) license (<http://creativecommons.org/licenses/by/4.0/>).